Journal of Materials Chemistry A

Accepted Manuscript

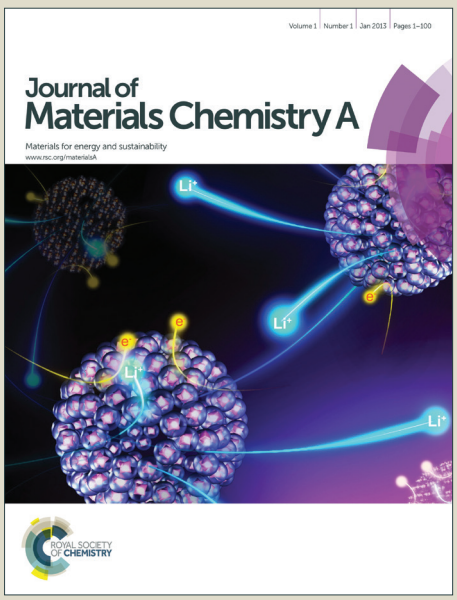

ROYAL SOCIETY OF CHEMISTRY

www.rsc.org/materialsA

Journal Name

RSCPublishing

COMMUNICATION

Constructing cubic-orthorhombic surface-phase junctions of $NaNbO_3$ towards significant enhancement of CO_2 photoreduction

Cite this: DOI: 10.1039/x0xx00000x

Peng Li,[a] Hua Xu,[b] Lequan Liu,[ad] Tetsuya Kako,[a] Naoto Umezawa,[abc] Hideki Abe[abc] and Jinhua Ye[*abd]

Received 00th January 2012,
Accepted 00th January 2012

DOI: 10.1039/x0xx00000x

www.rsc.org/

$NaNbO_3$ photocatalyst with cubic-orthorhombic surface-junctions was synthesized by a polymerized-complex method. Compared with cubic and orthorhombic $NaNbO_3$, the activity of mix-phase $NaNbO_3$ is enhanced by 30% and 200% in reducing CO_2 into CH_4, respectively. The enhancement of photoactivity over mix-phase $NaNbO_3$ was attributed to the cubic-orthorhombic surface-junctions which improved the charge separation.

Photocatalysis using semiconductor has attracted particular interests in the past decades because of its ability in directly converting the solar energy into chemical fuels.[1] The performances of photocatalyst are strongly affected by various parameters, such as crystallinity, surface area, surface state, and especially the crystal structure, which is usually the most important factor.[2] Generally, TiO_2 in anatase phase exhibits much better performances than those in the other phases in many photocatalytic reactions.[3] However, a commercial photocatalyst P25, which consists of anatase and rutile, shows higher activities than either pure anatase or rutile in water splitting and gaseous pollutant degradation.[4] In mixed-phase TiO_2, the previous reports revealed that the recombination of photo-generated electron-hole pairs in rutile is suppressed through electron transferring to lower energy anatase lattice trapping sites.[5] However, besides TiO_2, there are only a few reports about the mix-phase junction to enhance photocatalytic performance over the other semiconductors.[6]

Alkaline and alkaline earth metal niobate materials are typical environmentally friendly photocatalysts with high activities in water splitting because of their unique crystal structures containing a network of corner-shared octahedral units of $[NbO_6]$ metal cations, which enhance the charge migration in the crystals.[7] More recently, $NaNbO_3$ attracts extensive attentions due to its higher stability and narrower band gap than the other Nb-based photocatalysts.[8] In both of photocatalytic water splitting and CO_2 reduction, $NaNbO_3$ has the excellent performances.[9] Among a series of crystal structures, $NaNbO_3$ in cubic and orthorhombic phases are more important for photocatalysis as the cubic $NaNbO_3$ has the better activities and the orthorhombic NaNbO3 is the most stable phase at room temperature.[10]

In this study, the $NaNbO_3$ samples were synthesized from 400 to 600°C based on the polymerized complex method. Pure cubic and orthorhombic $NaNbO_3$ were respectively obtained at 400 and 600°C, while the $NaNbO_3$ samples with mixed phases were formed at the temperature ranging from 400 to 600°C. The crystal structures, optical properties, and microstructures of the prepared materials were differentiated by X-ray diffractometer (XRD) combined with ultraviolet-visible (UV-vis) spectroscopy and high-resolution transmission electron microscopy (HR-TEM). The photocatalytic performances of the $NaNbO_3$ samples were evaluated by CO_2 reduction in gaseous phase. Compared with pure cubic and orthorhombic $NaNbO_3$, the $NaNbO_3$ samples in mixed phases showed the enhanced activities. The surface junction between cubic and orthorhombic $NaNbO_3$ plays a significant role to enhance the separation of electron-hole pairs and therefore improve the photocatalytic performances.

According to the thermo-gravimetric/differential thermal analyzer (TG/DTA) measurement (as shown in Fig. S1), the polymerized precursor was selectively oxidized at different temperatures for 10 hours (the final products were named as

$NaNbO_3$-T, where T is the calcination temperature in Celsius). The crystallographic phases of the as-prepared $NaNbO_3$ samples were determined by powder XRD patterns (Fig. 1a). Under the oxidation temperature of 400 and 600°C, the products crystallized in cubic (the space group *Pm-3m*) and orthorhombic (the space group *Pbcm*) phases, respectively, since all the observed peaks in the patterns could be well indexed to the standard database cards (JCPDS-075-2102 for the cubic phase and JCPDS-073-0803 for the orthorhombic phase). When the oxidation temperature increased from 400 to 600°C, the $NaNbO_3$ sample showed an obvious phase transition from cubic phase to orthorhombic phase. The contents of cubic and orthorhombic phases in the sequence of as-prepared $NaNbO_3$ samples were estimated by simulating the XRD pattern with standard cubic and orthorhombic crystal structures. Fig. 1b plots the content evolutions of the cubic and orthorhombic phases in the $NaNbO_3$ samples with the oxidation temperature increasing. As reported in our previous work, the formation of cubic $NaNbO_3$ was attributed to the surface coordinated carbonates, which are generated from the oxidation of surface coordinated polymer. The desorption of surface carbonate releases the $NaNbO_3$ surface and induces the growth of orthorhombic $NaNbO_3$ when the oxidation temperature rises from 400 to 600°C.[10(b)]

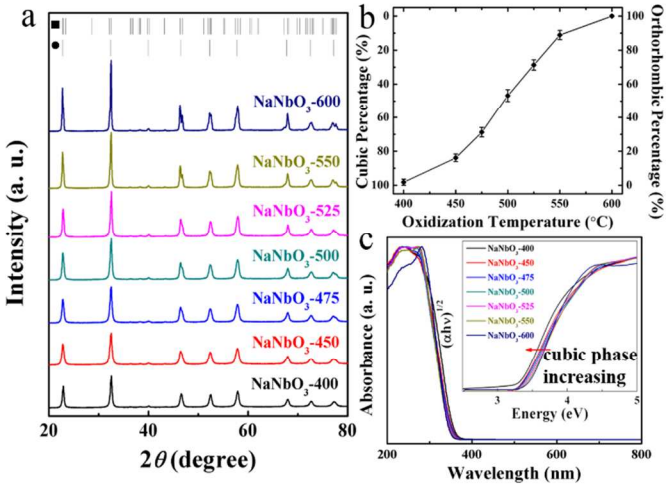

Fig. 1 (a) XRD patterns of the as-prepared $NaNbO_3$ samples. (■: orthorhombic; ●: cubic) (b) Dependence of cubic and orthorhombic $NaNbO_3$ contents on the oxidation temperature. (c) UV-Vis absorption spectra of the as-prepared $NaNbO_3$ samples and the inset in figure is the corresponding $(\alpha h\nu)^{1/2} \sim h\nu$ curves.

UV-visible absorption spectra of the $NaNbO_3$ powder samples prepared at various temperatures are shown in Fig. 1c. All the samples have the similar intense absorption edges appear in the UV region. Along with the phase transition from cubic phase to orthorhombic phase, the absorption edge of $NaNbO_3$ shows a slight and gradual blue shift, which is consistent with the previous report that cubic $NaNbO_3$ has a narrower band gap than orthorhombic $NaNbO_3$.[10] In the inset $(\alpha h\nu)^{1/2}$~energy plot, the band gaps of the as-prepared $NaNbO_3$ samples, which could be determined by recording the intercept, show the comprehensible change along with the oxidation temperature.

The process of crystal growth from cubic to orthorhombic $NaNbO_3$ was further studied by TEM measurement. The image of $NaNbO_3$-400 (as shown in Fig. 2a) shows that the cubic sample mainly contains ultrathin particles less than 10 nm. When the oxidation temperature increased to 600°C, the ultrathin particles grew into cuboid particles with the length of about 30 nm and the crystal has a transition from cubic to orthorhombic phase. However, if the oxidation temperature is between 400 and 600°C, the morphology is different from cubic and orthorhombic samples (TEM images supplied in the Supporting Information). In Fig. 2c, we clearly observe that two kinds of particles, the smaller ones less than 10 nm and the bigger ones about 30 nm, exist in the typical mix-phase sample $NaNbO_3$-475. Compared with the $NaNbO_3$-400 and $NaNbO_3$-600 samples, the two kinds of particles might be in cubic and orthorhombic phases, respectively, which could be further evidenced by the HR-TEM image (Fig. 2d). Therefore, the junctions between two kinds of particles are formed. Furthermore, because these junctions were generated in the phase-transition, the two phases contacted with each other closely, and can facilitate the charge transfer.

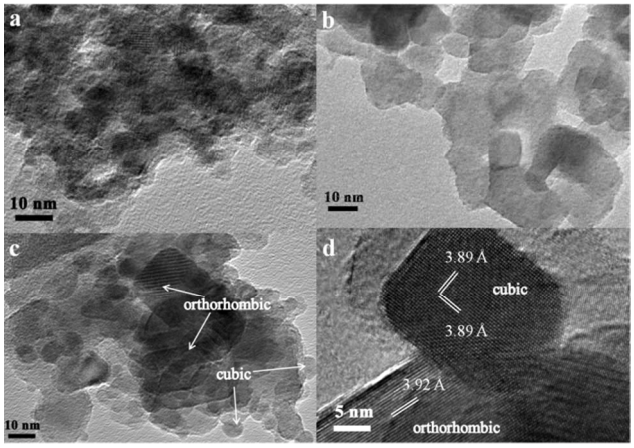

Fig. 2 TEM images of the $NaNbO_3$ samples oxidized at (a) 400°C, (b) 600°C and 475°C. (d) HR-TEM image of the $NaNbO_3$ sample oxidized at 475°C.

To assess the photocatalytic property of as-prepared $NaNbO_3$, the CO_2 photoreduction experiments were carried out in gaseous phase. Since in the gas-phase CO_2 photoreduction experiments, CH_4 is the main organic product, we measured the amounts of CH_4 evolution to judge the reaction activities. Fig. 3a exhibits the CH_4 evolutions over the series of $NaNbO_3$ samples (0.1 g) with 0.5 wt% Pt loading under the irradiation of full-arc Xe lamp (λ > 300 nm). All of the $NaNbO_3$ samples can reduce CO_2 into CH_4 under light irradiation but show different activities. For the pure phase $NaNbO_3$, the sample in cubic phase has the higher activity than that in orthorhombic phase, and the samples in mix-phase prepared between 450 and 525°C show better performance than the pure cubic or orthorhombic sample. The higher activities of mix-phase samples were also observed in photocatalytic water splitting (Supporting Information). Because the surface area is an important factor in gaseous CO_2 photoreduction, the surface-area specific rates of CH_4 evolution over the $NaNbO_3$ samples in 8 hours were calculated and are

shown in Fig. 3b. Different from the total CH_4 evolution, $NaNbO_3$-525 has the highest efficiency in reducing CO_2 into CH_4. This difference is attributed to the rapid decrease of surface area along with the oxidation temperature increasing from 400 to 600°C. However, all the mix-phase samples are still more efficient in CO_2 reduction than the two pure phases. A reference isotope experiment over $NaNbO_3$-500 was carried out in the present of D_2O to verify the source of hydrogen in the product. The GC-MS spectrum (as shown in Fig. S5) shows that CD_4 is the majority in the CH_4 product. Combined with our previous isotope experiment using $^{13}CO_2$ as a carbon source,[10(b)] the CH_4 molecules are generated from CO_2 and H_2O.

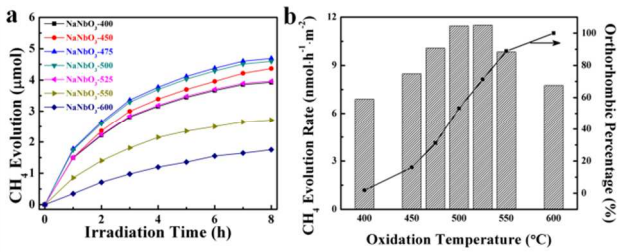

Fig. 3 (a) CH_4 evolution in gaseous phase reaction over the as-prepared $NaNbO_3$ samples with 0.5 wt% Pt loading under the irradiation of 300 W Xe lamp (λ > 300 nm). (b) The surface-area specific CH_4 evolution rates over the as-prepared $NaNbO_3$ samples.

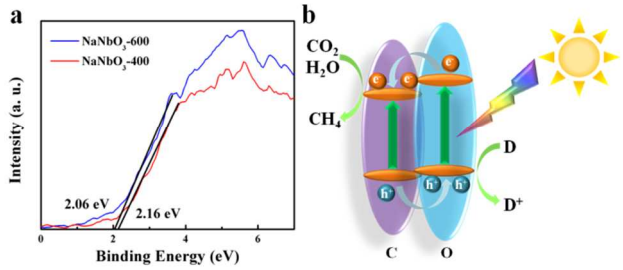

Fig. 4 (a) Valence band XPS curves of $NaNbO_3$-400 and $NaNbO_3$-600. (b) The proposed electron transfer in cubic-orthorhombic junctions and the surface photocatalytic reactions. (C: cubic $NaNbO_3$, O: orthorhombic $NaNbO_3$, D: electron donor)

The junctions between two phases could promote the spatial charge separation in the surface region, and the surface-phase junctions between anatase and rutile particles, which are formed in P25, are responsible to its high photocatalytic activity.[10] The same charge transfer process may also happen in the mix-phase $NaNbO_3$ photocatalysts. In other words, the formation of cubic-orthorhombic phase junctions can improves the photocatalytic performances of $NaNbO_3$. Our previous investigation proved that due to the asymmetric reformation of [NbO_6] octahedral ligand field, the energy level of the O 2*p* orbitals raises, which induces the larger band gap of orthorhombic $NaNbO_3$ and the higher energy levels of valence band (VB) and conduction band (CB) in orthorhombic $NaNbO_3$.[9] To confirm the electronic structural differences between cubic and orthorhombic $NaNbO_3$, VBs of $NaNbO_3$-400 and $NaNbO_3$-600 were measured by X-ray photoelectron spectroscopy (XPS). As shown in Fig 4a, the energy level of VB top in $NaNbO_3$-600 is 0.1 eV higher than that in $NaNbO_3$-400. From Fig. 1c, the band gaps of pure cubic and orthorhombic $NaNbO_3$ are determined as 3.27 and 3.43 eV, respectively. Thus, it can be deduced that the energy level of CB bottom in orthorhombic is 0.26 eV higher than that in cubic $NaNbO_3$, which thus induces the charge separation similar to P25. Fig. 4b plots the proposed electron transfer mechanism in cubic-orthorhombic junctions and the surface photocatalytic reactions. The phase junctions between cubic and orthorhombic $NaNbO_3$ can facilitate the transfer of the photo-excited electrons from the conduction band of the orthorhombic phase to the trapping sites on the cubic surface, thus avoiding the electron-hole recombination in orthorhombic $NaNbO_3$ and improving the charge separation efficiency in the mix-phase $NaNbO_3$ samples. Since the charge migration in cubic $NaNbO_3$ is easier than in orthorhombic $NaNbO_3$ and the photocatalytic activities over cubic $NaNbO_3$ is significantly higher than those over orthorhombic $NaNbO_3$,[10(a)] the enhanced photocatalytic performances over the mix-phase $NaNbO_3$ are understandable. After all, this obvious increase in the photocatalytic activity can be attributed to the formation of the surface cubic-orthorhombic junctions.

In conclusion, this work demonstrates that the photocatalytic activities of $NaNbO_3$ are greatly affected by the crystal structure, which can be selectively synthesized by a simple low temperature oxidation with the surface organic ligands assisted. More interestingly, the activities of photocatalytic CO_2 reduction and H_2 evolution could be greatly enhanced by forming the surface-phase junctions between the cubic and orthorhombic $NaNbO_3$ nanoparticles. The results and discussion in this study reveal that the surface/interface engineering of semiconductor photocatalyst is a feasible and efficient approach to promote the photocatalytic performance.

Notes and references

a Catalytic Materials Group, Environmental Remediation Materials Unit, National Institute for Materials Science (NIMS), 1-1 Namiki, Tsukuba, Ibaraki 305-0044, Japan
E-mail:Jinhua.YE@nims.go.jp
b TU-NIMS Joint Research Center, School of Materials Science and Engineering, Tianjin University, 92 Weijin Road, Nankai District, Tianjin, P. R. China
c PRESTO, Japan Science and Technology Agency (JST), 4-1-8 Honcho Kawaguchi, Saitama 332-0012, Japan
d International Center for Materials Nanoarchitectonics (WPI-MANA), National Institute for Materials Science (NIMS), 1-1 Namiki, Tsukuba, Ibaraki 305-0044, Japan

Acknowledgement: This work was partially supported by the World Premier International Research Center Initiative on Materials Nanoarchitectonics, MEXT, Japan.

Electronic Supplementary Information (ESI) available: [details of any supplementary information available should be included here]. See DOI: 10.1039/c000000x/

1 (a) H. Tong, S. X. Ouyang, Y. P. Bi, N. Umezawa, M. Oshikiri and J. H. Ye, *Adv. Mater.*, 2012, **24**, 229-251; (b) M. R. Hoffmann, S. T. Martin, W. Y. Choi and D. W. Bahnemann, *Chem. Rev.*, 1995, **95**, 69-96.

2 (a) A. Fujishima, X. T. Zhang and D. A. Tryk, *Surf. Sci. Rep.*, 2008, **63**, 515-582; (b) A. L. Linsebigler, G. Q. Lu and J. T. Yates, *Chem. Rev.*, 1995, **95**, 735-758; (c) G. Liu, J. C. Yu, G. Q. Lu and H. M. Cheng, *Chem. Commun.*, 2011, **47**, 6763-6783.

3 (a) G. Liu, C. H. Sun, H. G. Yang, S. C. Smith, L. Z. Wang, G. Q. Lu and H. M. Cheng, *Chem. Commun.*, 2010, **46**, 755-757; (b) M. Ni, M. K. H. Leung, D. Y. C. Leung and K. Sumathy, *Renew. Sust. Energ. Rev.*, 2007, **11**, 401-425

4 (a) M. A. Henderson, *Surf. Sci. Rep.*, 2011, **66**, 185-297; (b) O. Carp, C. L. Huisman and A. Reller, Prog. *Solid State Chem.*, 2004, **32**, 33-177.

5 (a) D. C. Hurum, A. G. Agrios, K. A. Gray, T. Rajh and M. C. Thurnauer, *J. Phys. Chem. B*, 2003, **107**, 4545-4549; (b) T. Kawahara, Y. Konishi, H. Tada, N. Tohge, J. Nishii and S. Ito, *Angew. Chem., Int. Ed.*, 2002, **41**, 2811-2813.

6 (a) T. Kako and J. Ye, *J. Mol. Catal. A: Chem.*, 2010, **320**, 79-84; (b) X. Wang, Q. Xu, M. R. Li, S. Shen, X. L. Wang, Y. C. Wang, Z. C. Feng, J. Y. Shi, H. X. Han and C. Li, *Angew. Chem., Int. Ed.*, 2012, **51**, 13089-13092.

7 (a) T. Takata, A. Tanaka, M. Hara, J. N. Kondo and K. Domen, *Catal. Today*, 1998, **44**, 17-26; (b) K. Tanabe, *Catal. Today*, 2003, **78**, 65-77; (c) A. S. Dias, S. Lima, D. Carriazo, V. Rives, M. Pillinger and A. A. Valente, *J. Catal.*, 2006, **244**, 230-237

8 K. Maeda, *J Photoch Photobio C*, 2011, **12**, 237-268.

9 (a) H. F. Shi, X. K. Li, D. F. Wang, Y. P. Yuan, Z. G. Zou and J. H. Ye, *Catal. Lett.*, 2009, **132**, 205-212; (b) K. Saito and A. Kudo, *Inorg. Chem.*, 2010, **49**, 2017-2019; (c) H. F. Shi, T. Z. Wang, J. Chen, C. Zhu, J. H. Ye and Z. G. Zou, *Catal. Lett.*, 2011, **141**, 525-530.

10 (a) P. Li, S. X. Ouyang, G. C. Xi, T. Kako and J. H. Ye, *J. Phys. Chem. C*, 2012, **116**, 7621-7628; (b) P. Li, S. Ouyang, Y. Zhang, T. Kako and J. Ye, *J. Mater. Chem. A*, 2013, **1**, 1185-1191.

11 J. Zhang, Q. Xu, Z. Feng, M. Li and C. Li, *Angew. Chem., Int. Ed.*, 2008, **47**, 1766-1769.

